Sensors and Materials, Vol. 36, No. 5 (2024) 1849–1858
MYU Tokyo

S & M 3639

Time-resolved Response Improvement of Oxygen-doped a-In–Ga–Sn–O Metal–Semiconductor–Metal Photodetectors by Sputtering

Artde Donald Kin-Tak Lam,[1] Tsung-I Liao,[2]
Sheng-Po Chang,[3*] and Shoou-Jinn Chang[2,4]

[1]School of Design & Straits College of Engineering, Fujian University of Technology
No. 3 Xueyuan Road, University Town, Fuzhou City, Fujian Province, China
[2]Program on Semiconductor Manufacturing Technology, Academy of Innovative Semiconductor and Sustainable Manufacturing, National Cheng Kung University, Tainan City 70101, Taiwan
[3]Department of Microelectronics Engineering, National Kaohsiung University of Science and Technology, Kaohsiung City 811, Taiwan
[4]Institute of Microelectronics & Department of Electrical Engineering, National Cheng Kung University, Tainan City 70101, Taiwan

(Received October 30, 2023; accepted April 15, 2024)

Keywords: transparent oxide semiconductors, indium gallium tin oxide, UV photodetectors, reactive sputtering, oxygen doping

In this work, we fabricated indium gallium zinc oxide (IGTO) metal–semiconductor–metal (MSM) photodetectors (PDs) with different oxygen flow ratios and investigated and discussed their characteristics. 0% PDs show a high responsivity of 25.75 A/W, but their dark current is very high and their switching time is low. 10% PDs exhibit the highest performance. They show a high photo/dark current ratio of 1.05×10^5 with a low dark current of 1.19×10^{-11} A. Their responsivity is 0.12 A/W and their rejection ratio is 9.38×10^5, which is sufficiently high to ensure the accuracy of distinguishing between UV and visible ranges. Their rising time is 206 s and their falling time is 58 s. It was observed that the response time shortened as the oxygen flow ratio was increased.

1. Introduction

Transparent oxide semiconductors (TOSs) have attracted considerable attention owing to their various applications, including, but not limited to, LEDs, photosensors, and resistive random-access memory. The materials commonly used in TOSs include indium oxide (In_2O_3),[1–3] gallium oxide (Ga_2O_3),[3,4] tin oxide (SnO_2),[5,6] zinc oxide (ZnO),[7–11] indium gallium oxide (IGO),[12,13] indium tin oxide (ITO),[14] and indium gallium zinc oxide (IGZO).[15–18] These materials are recognized for their exceptional electrical conductivity, excellent optical transparency in the visible wavelength, and wide bandgap.[19,20]

*Corresponding author: e-mail: changsp@nkust.edu.tw
https://doi.org/10.18494/SAM4803

ISSN 0914-4935
https://myukk.org/

UV photodetectors (PDs) have attracted considerable attention because of their wide range of applications in civilian infrastructure, military facilities, and optoelectrical circuits.[21–23] Moreover, the UV PD with a cut-off wavelength from 200 to 280 nm is considered as solar-blind since solar radiation in this range cannot penetrate Earth's atmosphere. Hence, solar-blind UV PDs with good stability have a variety of applications such as the inspection of UV leakage, biochemical detection, and ozone hole monitoring.[24]

A wide bandgap Is required to obtain a low cut-off wavelength. As one of the wide-bandgap semiconductors, Ga_2O_3 is a good choice owing to its wide bandgap of 4.9–5.3 eV, and it shows great responsivity in the UV range.[25,26] However, to increase the carrier density and obtain high-response UV single-crystal β-Ga_2O_3, a high-temperature process is unavoidable.[27] Thus, a Ga_2O_3-based compound becomes a potential material. We can deposit a Ga_2O_3-based compound by sputtering at room temperature if we add other materials of high carrier density such as In_2O_3[28,29] and SnO_2.[30,31] In this work, the fabrication of IGTO UV PDs based on the metal–semiconductor–metal (MSM) structure was demonstrated. The effects of different oxygen flow ratios, optical characteristics, and electrical analysis were discussed.

2. Experiment

First, 2 × 2 cm^2 quartz substrates were cleaned with acetone, isopropyl alcohol, and deionized (DI) water in an ultrasonic bath in this order. Then, 150-nm-thick IGTO films were subsequently deposited by RF-magnetron sputtering from the composite IGTO target (In_2O_3:Ga_2O_3:SnO_2 = 1:1:1 mol) with an RF power of 80 W. The chamber pressure was maintained at 5 mTorr with three different oxygen flow ratios [O_2/(Ar + O_2)] of 0, 10, and 20%, along with a total gas flow rate of 50 sccm. Finally, 30-nm-thick Ni and 70-nm-thick Au with an interdigitated structure were deposited as the adhesion and contact layers, respectively, onto IGTO films by thermal evaporation. The width (W) and length (L) of the fingers are 0.1 and 1.2 mm, respectively, and the finger distance is 0.2 mm, as shown in Fig. 1.

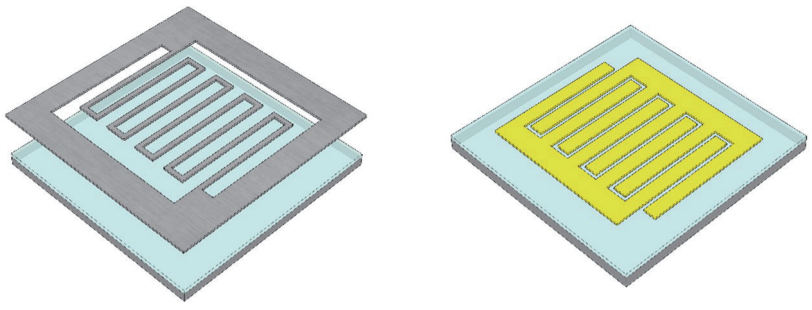

(a) (b)

Fig. 1. (Color online) (a) Metal mask of interdigitated electrodes and IGTO film on quartz. (b) Schematic of IGTO PD.

To characterize the electrical properties of the fabricated IGTO MSM PDs, we measured the devices in the dark and under illumination using a semiconductor parameter analyzer (model B1500A, Agilent Technologies) at room temperature and atmospheric pressure. The light source was a 150 W Xe lamp and a monochromator that covers the wavelength range from 200 to 800 nm. The power of the monochromator light was measured with Nova II P/N7Z01550.

3. Results and Discussion

Figure 2 shows that the IGTO thin films exhibit a high degree of optical transparency with an average transmittance of nearly 90% in the light wavelength range from 400 to 700 nm and a low transmittance in the ultraviolet region, especially in the UVC range. The optical bandgap for IGTO thin films can be obtained using the Tauc relation[32,33] as follows:

$$(\alpha h\upsilon)^n = A\left(h\upsilon - E_g\right), \tag{1}$$

where α is the absorption coefficient, h = 4.136 × 10^{-15} eV·s is Planck's constant, υ is the frequency of the incident photon, A is a constant, and E_g is the bandgap. For direct allowed transitions, n is typically 2, whereas for indirect allowed transitions, n is 0.5. In the case of IGTO, we assumed an n value of 2 because band-to-band transitions are allowed. The $(ah\upsilon)^n$ versus $h\upsilon$ curves were depicted so that we could obtain the bandgap from the x-axis intercept of the line, which is tangent to the inflection point. We used the Tauc plot method to determine the bandgap for samples with different oxygen flow ratios, as shown in Fig. 2. The optical bandgaps for samples with 0, 5, 10, and 20% oxygen flow ratios are 5.02, 5.01, 4.98, and 4.98 eV, respectively. This analysis reveals that variations in oxygen flow ratios have a negligible impact on the optical bandgap of IGTO.

The chemical bonding in IGTO thin films was studied by XPS, which is useful for detecting changes in oxygen vacancy content in IGTO thin films. Through Gaussian fitting, there are

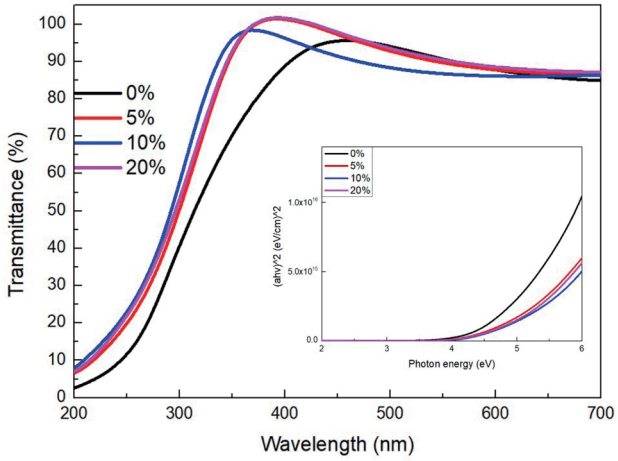

Fig. 2. (Color online) Transmittance spectra and Tauc plot of IGTO thin films.

three peaks that can be deconvoluted from the O 1s signal. The first peak at 530.1 ± 0.1 eV represents the well-bonded oxygen with a metal cation (O_I, M-O). The second peak at 531.5 ± 0.1 eV represents the oxygen vacancies (O_{II}, V_O). The third peak at 532.6 ± 0.1 eV represents the metal hydroxide species (O_{III}, M-OH). Subsequently, the areas under the curves of these three peaks were calculated and then compared with the total area to determine the proportions of O_I, O_{II}, and O_{III}. The proportion of O_{II}, which is specifically associated with oxygen vacancies, was obtained and is presented in Table 1 and Figs. 3(a)–3(d). Notably, the data indicates that as the oxygen flow ratio during the sputtering process is increased from 0 to 20%, the proportion of oxygen vacancies decreases from 49.9 to 34.9%. This demonstrates that supplying more oxygen during sputtering can effectively fill and compensate for oxygen vacancies. This, in turn, helps regulate the number of charge carriers and defects in the material.

Table 1
Proportion of O_{II} with different oxygen flow ratios.

Oxygen flow ratio (%)	0	5	10	20
O_{II}/O_{total} (%)	49.9	44.2	41.2	34.9

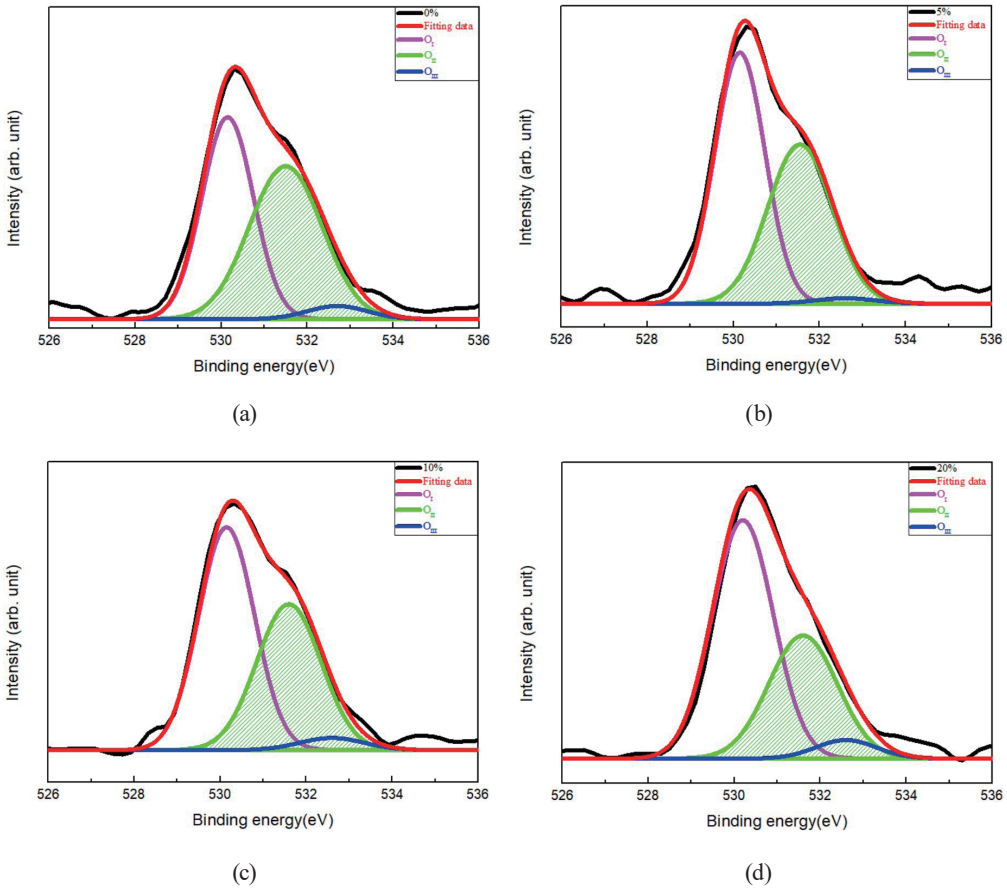

Fig. 3. (Color online) XPS spectra of O 1s core level of IGTO thin film as a function of oxygen partial pressure [(a) 0, (b) 5, (c) 10, and (d) 20%], which are deconvoluted into three peaks through Gaussian fitting.

To investigate the effect of oxygen flow ratio on IGTO, we fabricated IGTO MSM PDs as described above and measured them under certain conditions. The wavelength of the light source applied to devices is from 220 to 500 nm with an interval of 10 nm, and the bias applied to devices is from −10 to 10 V. The *I–V* characteristics of PDs with oxygen flow ratios of 0, 10, and 20% are shown in Fig. 4. From the results, we find that the dark current and photocurrent decreased as the oxygen flow ratios were increased, which is ascribed to higher Schottky barriers and the reduction of oxygen vacancies in IGTO. While the oxygen flow ratio is increased, oxygen vacancies may be filled by oxygen, which causes the low conductivity. This agrees with the results of XPS analyses and helps us realize different performance characteristics of devices by controlling the oxygen flow ratio. The dark currents of the 0, 10, and 20% PDs are 3.52×10^{-4}, 1.19×10^{-11}, and 6.42×10^{-12} A, respectively. The photocurrents under the light wavelength of 250 nm for the 0, 10, and 20% PDs are 6.20×10^{-4}, 1.25×10^{-6}, and 1.08×10^{-7} A, respectively.

We found that the 0% PDs are photoconductors. A good way to confirm the photoconductive gain existing in them is by determining the external quantum efficiency (*EQE*).[34,35] *EQE* is defined as the number of carriers circulating through a PD per adsorbed photon and per unit time. It can be expressed as[36]

$$EQE = \frac{hc}{e\lambda} \cdot \frac{\Delta I}{P} \cdot \frac{1}{G}, \tag{2}$$

where h is Planck's constant, c is the velocity of light, e is the electronic charge, λ is the wavelength of radiation, G is the photoconductive gain, and ΔI is the difference between photocurrent and dark current. The *EQE* of the 0% PDs applied to 10 V at the light wavelength of 250 nm is 99.7%.

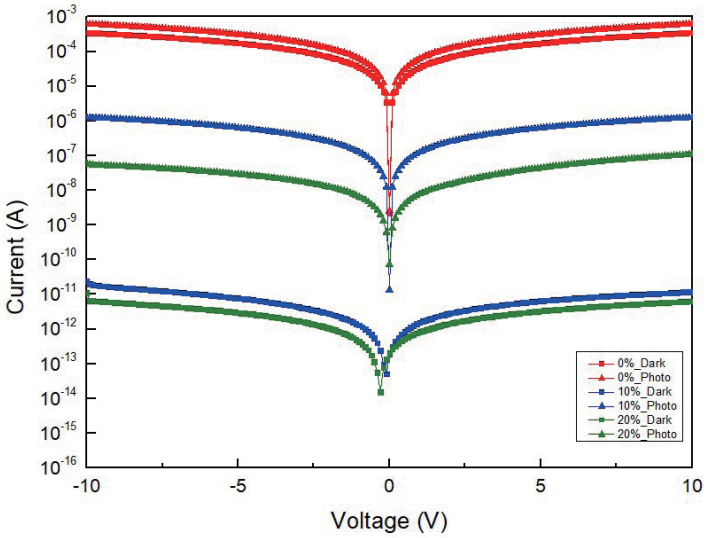

Fig. 4. (Color online) *I–V* characteristics of PDs with oxygen flow ratios of 0, 10, and 20%.

The responsivities from 250 to 500 nm with an interval of 10 nm for IGTO MSM PDs with different oxygen ratios are shown in Figs. 5(a)–5(c). The responsivities measured at 250 nm for PDs with oxygen flow ratios of 0, 10, and 20% are 25.75, 0.12, and 0.01 A/W, respectively. The *I-V* data, responsivity, and rejection ratio (*RR*) are summarized in Table 2. In this work, we define the UV-to-visible *RR* as the responsivity measured at 250 nm divided by that measured at 500 nm, as

$$RR = \frac{Responsivity(300\,\mathrm{nm})}{Responsivity(500\,\mathrm{nm})}. \tag{3}$$

The time-resolved response of IGTO MSM PDs is also discussed. The rising time can be defined as the time required for the current to increase from 10 to 90% of the peak value when continuously illuminated, whereas the falling time is that needed for the current to decay from 90 to 10% when the light resource is removed. The wavelength of light is 250 nm and the bias voltage applied to the devices is 10 V. All the devices were switched on and off for 5 cycles with an interval of 300 s. The photocurrent of the 0% PDs reached 4.34×10^{-4} A after the first interval of illumination. Nevertheless, it not only did not reach the saturation current, but also did not return to its initial value before illumination, as shown in Fig. 6(a). The 10 and 20% PDs exhibited shorter switching times than the 0% PDs, as depicted in Figs. 6(b) and 6(c); the average response times are listed in Table 3. We observed that the samples with high oxygen flow ratios showed faster switching responses. Because oxygen vacancies captured the electron–hole pairs excited by the illumination, it took a longer time to switch the devices. Thus, the 0% PDs cannot return to their initial dark current level since they need a longer recovery time instead of immediate recombination.[37–40]

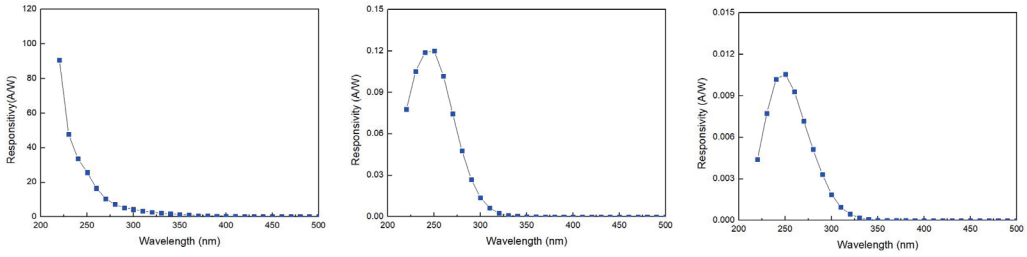

(a) (b) (c)

Fig. 5. (Color online) Responsivities of PDs with oxygen flow ratios of (a) 0, (b) 10, and (c) 20%.

Table 2
Characteristics of IGTO MSM PDs.

Oxygen flow ratio (%)	Photocurrent (A)	Dark current (A)	Photo/dark current ratio	Responsivity (A/W)	*RR*
0	6.20×10^{-4}	3.52×10^{-4}	1.76	25.75	367.86
10	1.25×10^{-6}	1.19×10^{-11}	1.05×10^{5}	0.12	9.38×10^{5}
20	1.08×10^{-7}	6.42×10^{-12}	1.68×10^{4}	0.01	4.13×10^{4}

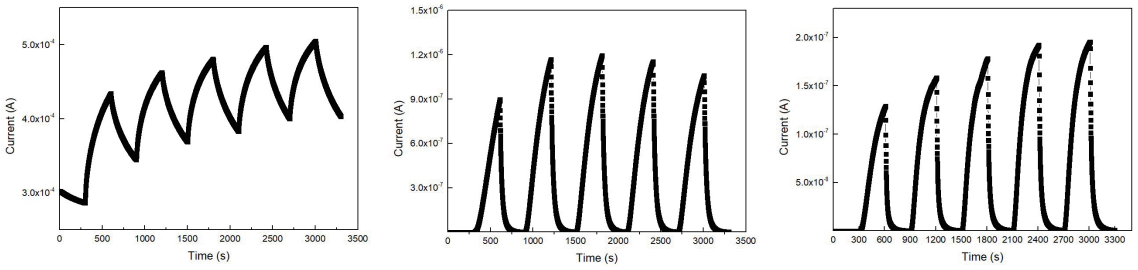

(a) (b) (c)

Fig. 6. Time-resolved responses of (a) 0, (b) 10, and (c) 20 PDs.

Table 3
Average response times of IGTO MSM PDs.

Oxygen flow ratio (%)	Rising time (s)	Falling time (s)
0	>300	>300
10	206	58
20	191	43

4. Conclusions

The results demonstrated that IGTO thin films exhibit excellent transparency in the visible range while effectively blocking UVC light. The optical bandgap of IGTO was found to be consistent across different oxygen flow ratios. XPS analysis revealed changes in oxygen vacancy content in IGTO films, demonstrating that supplying more oxygen during sputtering can effectively fill and compensate for oxygen vacancies. This was confirmed through the analysis of the *I–V* characteristics and responsivity spectra of IGTO MSM PDs.

Moreover, we investigated the time-resolved response of the PDs. The results showed that samples with higher oxygen flow ratios had faster swtching responses, primarily attributed to the electron trapping induced by oxygen vacancies.

Acknowledgments

The authors would like to thank the National Science and Technology Council, Taiwan, for financially supporting this research under Contract Nos. NSTC 112-2221-E-006-117-MY3 and 112-2218-E-006-010-MBK. The authors gratefully acknowledge the use of JEOL JEM-2100F CS STEM equipment belonging to the Instrument Center of National Cheng Kung University.

References

1 G. Cai, Z. Chen, L. Qiang, B. Yan, Y. Zhuo, J. Lin, X. Wang, Y. Pei, and G. Wang: Jpn. J. Appl. Phys. **57** (2018) 110301. https://doi.org/10.7567/JJAP.57.110301
2 H.-L. Zhao, F. Shan, X.-L. Wang, J.-Y. Lee, and S.-J. Kim: IEEE J. Electron Devices Soc. **10** (2022) 379. https://doi.org/10.1109/JEDS.2022.3170111
3 T. Oshima, T. Okuno, and S. Fujita: Jpn. J. Appl. Phys. **46** (2007) 7217. https://doi.org/10.1143/JJAP.46.7217

4 M. I. Pintor-Monroy, M. G. Reyes-Banda, C. Avila-Avendano, and M. A. Quevedo-Lopez: IEEE Sens. J. **21** (2021) 14807. https://doi.org/10.1109/JSEN.2021.3074623
5 Y. Ugai, T. Yukawa, Y. H. Y. Hatta, and S. A. S. Aoki: Jpn. J. Appl. Phys. **35** (1996) L1027. https://doi.org/10.1143/JJAP.35.L1027
6 C. W. Shih, A. Chin, C. F. Lu, and W. F. Su: IEEE Electron Device Lett. **40** (2019) 909. https://doi.org/10.1109/LED.2019.2912032
7 D. A. Mourey, D. A. Zhao, and T. N. Jackson: IEEE Electron Device Lett. **31** (2010) 326. https://doi.org/10.1109/LED.2010.2041424
8 Y.-L. Chu, Y.-H. Liu, T.-T. Chu, and S.-J. Young: IEEE Sens. J. **22** (2022) 5644. https://doi.org/10.1109/JSEN.2022.3150254
9 Y.-L. Chu, S.-J. Young, Y.-J. Chu, Y.-H. Liu, and T.-T. Chu: IEEE Electron Device Lett. **44** (2022) 124. https://doi.org/10.1109/LED.2022.3220753
10 Y.-L. Chu, S.-J. Young, T.-T. Chu, A. Khosla, K.-Y. Chiang, and L.-W. Ji: ECS J. Solid State Sci. Technol. **10** (2021) 127001. https://doi.org/10.1149/2162-8777/ac3e43
11 Y.-L. Chu, S.-J. Young, L.-W. Ji, I.-T. Tang, and T.-T. Chu: Sensors **20** (2020) 3861
12 F. He, Y. Wang, H. Yuan, Z. Lin, J. Su, J. Zhang, J. Chang, and Y. Hao: Ceram. Int. **47** (2021) 35029. https://doi.org/10.1016/j.ceramint.2021.09.044
13 Y.-C. Cheng, S.-P. Chang, and S.-J. Chang: Mater. Res. Express **6** (2019) 106445. https://doi.org/10.1088/2053-1591/ab24a6
14 H. Ferhati and F. Djeffal: IEEE Sens. J. **19** (2019) 7942. https://doi.org/10.1109/JSEN.2019.2920815
15 C. Chiu, W. Weng, S. Chang, S.-P. Chang, and T. Chang: IEEE Sens. J. **11** (2011) 2902. https://doi.org/10.1109/JSEN.2011.2146770
16 E. Chong, Y. S. Chun, S. H. Kim, and S. Y. Lee: J. Electr. Eng. Technol. **6** (2011) 539. https://doi.org/10.5370/JEET.2011.6.4.539
17 S. Kim, Y. W. Jeon, Y. Kim, D. Kong, H. K. Jung, M.-K. Bae, J.-H. Lee, B. Du Ahn, S. Y. Park, and J.-H. Park: IEEE Electron Device Lett. **33** (2011) 62. https://doi.org/10.1109/LED.2011.2173153
18 H. Yabuta, M. Sano, K. Abe, T. Aiba, T. Den, H. Kumomi, K. Nomura, T. Kamiya, and H. Hosono: Applied Phys. Lett. **89** (2006) 112123. https://doi.org/10.1063/1.2353811
19 Y. Hara, T. Kikuchi, H. Kitagawa, J. Morinaga, H. Ohgami, H. Imai, T. Daitoh, and T. Matsuo: J. Soc. Inf. Disp. **26** (2018) 169. https://doi.org/10.1002/jsid.648
20 S. Nakano, N. Saito, K. Miura, T. Sakano, T. Ueda, K. Sugi, H. Yamaguchi, I. Amemiya, M. Hiramatsu, and A. Ishida: J. Soc. Inf. Disp. **20** (2012) 493. https://doi.org/10.1002/jsid.111
21 H. K. Yadav, K. Sreenivas, and V. Gupta: Appl. Phys. Lett. **90** (2007) 172113. https://doi.org/10.1063/1.2733628
22 W. Wang, X. Pan, W. Dai, Y. Zeng, and Z. Ye: RSC Adv. **6** (2016) 32715. https://doi.org/10.1039/C6RA02924H
23 T. Oshima, T. Okuno, and S. Fujita: Jpn. J. Appl. Phys. **48** (2009) 120207. https://doi.org/10.1143/JJAP.48.120207
24 X. Chen, F. Ren, S. Gu, and J. Ye: Photonics Res. **7** (2019) 381. https://doi.org/10.1364/PRJ.7.000381
25 K. Akaiwa and S. Fujita: Jpn. J. Appl. Phys. **51** (2012) 070203. https://doi.org/10.1143/JJAP.51.070203
26 A. Kuramata, K. Koshi, S. Watanabe, Y. Yamaoka, T. Masui, and S. Yamakoshi: Jpn. J. Appl. Phys. **55** (2016) 1202A2. https://doi.org/10.7567/JJAP.55.1202A2
27 S. Han, X. Huang, M. Fang, W. Zhao, S. Xu, D. Zhu, W. Xu, M. Fang, W. Liu, and P. Cao: J. Mater. Chem. C. **7** (2019) 11834. https://doi.org/10.1039/C9TC03613J
28 T.-H. Chang, S.-J. Chang, W.-Y. Weng, C.-J. Chiu, and C.-Y. Wei: IEEE Photonics Technol. Lett. **27** (2015) 2083. https://doi.org/10.1109/LPT.2015.2453317
29 K.-Y. Chen, C.-C. Hsu, H.-C. Yu, Y.-M. Peng, C.-C. Yang, and Y.-K. Su: IEEE Trans. Electron Devices **65** (2018) 1817. https://doi.org/10.1109/TED.2018.2817637
30 A. Mondal, M. K. Yadav, S. Shringi, and A. Bag: Nanotechnology **31** (2020) 294002. https://doi.org/10.1088/1361-6528/ab82d4
31 M.-M. Fan, Y.-J. Lu, K.-L. Xu, Y.-X. Cui, L. Cao, and X.-Y. Li: Appl. Surf. Sci. **509** (2020) 144867. https://doi.org/10.1016/j.apsusc.2019.144867
32 F. Shan, B. Shin, S. Jang, and Y. Yu: J. Eur. Ceram. Soc. **24** (2004) 1015. https://doi.org/10.1016/S0955-2219(03)00397-2
33 M. G. Yun, S. H. Kim, C. H. Ahn, S. W. Cho, and H. K. Cho: J. Phys. D: Appl. Phys. **46** (2013) 475106. https://doi.org/10.1088/0022-3727/46/47/475106
34 B. Cheng, J. Xu, Z. Ouyang, X. Su, Y. Xiao, and S. Lei: J. Mater. Chem. C. **2** (2014) 1808. https://doi.org/10.1039/C3TC32059F
35 S. Han, Z. Zhang, J. Zhang, L. Wang, J. Zheng, H. Zhao, Y. Zhang, M. Jiang, S. Wang, and D. Zhao: Appl. Phys. Lett. **99** (2011) 242105. https://doi.org/10.1063/1.3670334

36 L. Hu, J. Yan, M. Liao, L. Wu, and X. Fang: Small **7** (2011) 1012. https://doi.org/10.1002/smll.201002379
37 P. Wu, J. Zhang, J. Lu, X. Li, C. Wu, R. Sun, L. Feng, Q. Jiang, B. Lu, and X. Pan: IEEE Trans. Electron Devices **61** (2014) 1431. https://doi.org/10.1109/TED.2014.2312947
38 J. Wang, Y. Xiong, L. Ye, W. Li, G. Qin, H. Ruan, H. Zhang, L. Fang, C. Kong, and H. Li: Opt. Mater. **112** (2021) 110808. https://doi.org/10.1016/j.optmat.2021.110808
39 J.-S. Jheng, C.-K. Wang, Y.-Z. Chiou, S.-P. Chang, and S.-J. Chang: Coatings **10** (2020) 994. https://doi.org/10.3390/coatings10100994
40 Z. Han, H. Liang, W. Huo, X. Zhu, X. Du, and Z. Mei: Adv. Opt. Mater. **8** (2020) 1901833. https://doi.org/10.1002/adom.201901833

About the Authors

Artde Donald Kin-Tak Lam received his B.S. degree in mechanical engineering from National Cheng Kung University (Tainan, Taiwan) in 1987 and his Ph.D. degree in electromechanical and mechanical engineering from National Sun Yat-Sen University (Kaohsiung, Taiwan) in 1993. He is a full professor in the School of Design & Straits College of Engineering of Fujian University of Technology, China. His research areas include MEMS, man–machine interfaces, and sensors.

Tsung-I Liao received his B.S. degree from National Cheng Kung University, Taiwan (R.O.C.). He is now studying for his Ph.D. degree at the Academy of Innovative Semiconductor and Sustainable Manufacturing of the same university. His research interests are in GaN HEMT and GaN-based sensors.

Sheng-Po Chang received his B.S. degree in electronic engineering from Southern Taiwan University of Science and Technology, Tainan, Taiwan, in 2004, his M.S. degree in nanotechnology and microsystems engineering, and his Ph.D. degree in microelectronics, both from National Cheng Kung University (NCKU), Tainan, in 2006 and 2009, respectively. He is currently an assistant professor at the Department of Microelectronics Engineering, National Kaohsiung University of Science and Technology. His current research interests include II–VI and III–V optoelectronic devices, semiconductor physics, solar cells, and nanotechnology.

Shoou-Jinn Chang received his B.S. degree from National Cheng Kung University (NCKU), Tainan, Taiwan, in 1983, his M.S. degree from the State University of New York, Stony Brook, NY, USA, in 1985, and his Ph.D. degree from the University of California, Los Angeles, CA, USA, in 1989, all in electrical engineering. From 1989 to 1992, he was a research scientist at Nippon Telegraph and Telephone Basic Research Laboratories, Musashino, Tokyo, Japan. He joined the Department of Electrical Engineering, NCKU, in 1992 as an associate professor, where he was promoted to a full professor in

1998. He served as the Director of the Institute of Microelectronics, NCKU from August 2008 to July 2011, and the Deputy Director of the Center for Micro/Nano Science and Technology, NCKU from February 2006 to January 2011. He is currently the Deputy Director of the Advanced Optoelectronic Technology Center, NCKU. From January to March 1999, he was a Royal Society Visiting Scholar at the University of Wales, Swansea, U.K.; from July 1999 to February 2000, he was a Visiting Scholar at the Research Center for Advanced Science and Technology, University of Tokyo, Tokyo, Japan; from August to September 2001, he was a Visiting Scholar at the Institute of Microstructural Science, National Research Council, Canada; from August to September 2002, he was a Visiting Scholar at the Institute of Physics, Stuttgart University, Stuttgart, Germany; and from July to September 2005, he was a Visiting Scholar at the Faculty of Engineering, Waseda University, Tokyo. He is also an Honorary Professor at Changchun University of Science and Technology, China. His current research interests include semiconductor physics, optoelectronic devices, and nanotechnology. Dr. Chang received the Outstanding Research Award from the National Science Council, Taiwan, in 2004. He is a Fellow of the Optical Society of America (OSA), the International Society for Optical Engineers (SPIE), and the Institute of Electrical and Electronics Engineers (IEEE).